Akhilesh K. Jha
Graduate Student

Daniel J. Inman*
G. R. Goodson Professor and Director,
Fellow ASME

Center for Intelligent Material Systems
and Structures,
Virginia Polytechnic Institute and
State University,
Blacksburg, VA 24061-0105

Raymond H. Plaut
D. H. Pletta Professor,
Fellow ASME
Charles E. Via, Jr. Department of Civil
and Environmental Engineering,
Virginia Polytechnic Institute and
State University,
Blacksburg, VA 24061-0105

Free Vibration Analysis of an Inflated Toroidal Shell

Free vibration analysis of a free inflated torus of circular cross-section is presented. The shell theory of Sanders, including the effect of pressure, is used in formulating the governing equations. These partial differential equations are reduced to ordinary differential equations with variable coefficients using complete waves in the form of trigonometric functions in the longitudinal direction. The assumed mode shapes are divided into symmetric and antisymmetric groups, each given by a Fourier series in the meridional coordinate. The solutions (natural frequencies and mode shapes) are obtained using Galerkin's method and verified with published results. The natural frequencies are also obtained for a circular cylinder with shear diaphragm boundary condition as a special case of the toroidal shell. Finally, the effects of aspect ratio, pressure, and thickness on the natural frequencies of the inflated torus are studied. [DOI: 10.1115/1.1467650]

1 Introduction

Use of an inflated structure in an aerospace application goes back to the early 1960's and the ECHO series of satellites (Malone and Crawford [1]). Inflatable structures have been the subject of renewed interest in recent years for space applications such as communication antennas, solar thermal propulsion, and space solar power. The major advantages of using inflatable structures in space are their extremely low weight, on-orbit deployability, and subsequent space saving in launching. An inflated torus is a key component of many inflated structure designs (Dornheim [2]) that serves as structural support for optical systems such as a thin membrane reflector or a Fresnel lens. In the design of thin elastic shell structures, it is important to know their dynamic behavior as well as their load carrying ability. The dynamic behavior is particularly important for satellite structures since they are subjected to a variety of time-varying loadings. The free vibration study is needed in order to obtain the natural frequencies and the mode shapes, which are required for the forced vibration analysis.

Free vibration of toroidal shells without pressure has been studied by many researchers, for example, Kordes [3], McGill [4], Kosawada et al. [5], Fang [6], and Leung and Kwok [7]. However, there have been few studies on the toroidal shell subjected to pressure. Jordan [8] predicted the vibratory frequencies using the Rayleigh quotient and performed experiments. Saigal et al. [9] found an analytical solution of a prestressed toroidal membrane with fixed boundary conditions. He assumed that the in-plane displacement components are zero and the radius of the torus is very large compared to the radius of its cross-section. The results are valid only for a special case of a torus due to the strong assumptions made in order to simplify the governing equations. Plaut et al. [10] used shell theory for an inflatable arch with fixed boundary conditions to find the deflections when subjected to snow and wind loadings. However, they did not perform the free vibration analysis. Liepins [11] presented free vibration analysis of a toroidal membrane under internal pressure. He solved the governing equations using a finite difference method and obtained the frequencies and mode shapes by a trial and error method in the Holzer fashion. Lewis [12] analyzed an inflated toroidal structure using finite element analysis. This work uses Galerkin's method along with Fourier series, rather than the finite difference method or the finite element method, for the free vibration analysis of an inflated toroidal shell.

The goal of the present paper is to perform a free vibration analysis of an inflated torus with free boundary conditions. It is assumed that the cross-section is circular, the thickness is uniform, and the material is linearly elastic and isotropic. We assume that the pressure remains constant while the torus is vibrating. We use a modified Sanders' shell theory (Sanders [13], Budiansky [14]). Modifications involve inclusions of the geometric nonlinearity in the in-plane strains in conjunction with prestresses. Consideration of geometric nonlinearity is important in order to capture the effects of pressure. The nonlinearity is considered only with the prestresses so that the resulting vibration equations are linear. The bending rigidity of the shell is not assumed to be negligible, and this implies that the method is valid for a large class of shells. Initial stresses are assumed to be membrane in nature, i.e., uniform throughout the thickness of the shell.

First, the toroidal shell geometry is described and the initial stresses due to internal pressure are obtained. Thereafter, the equations of motion are presented. Since it is very difficult to solve the governing partial differential equations exactly, we use the Galerkin's method. The governing equations are reduced to ordinary differential equations with variable coefficients using complete waves in the form of sine and cosine functions in the longitudinal direction and an arbitrary periodic function in the meridional direction. Then this arbitrary meridional function is explicitly written in two separate groups to demonstrate the independent symmetric and antisymmetric modes of vibration using Fourier series. We also describe the procedure to derive the standard eigenvalue problem, which provides the natural frequencies and mode shapes. First, a special case of circular cylinder without pressure is considered. Thereafter, the inflated torus is analyzed. In both cases, the results are compared with published ones. A detailed analysis of mode shapes and natural frequencies is presented for an inflated torus with free boundary conditions.

*Corresponding author. Ph.: +1-540-231-4709, Fax: +1-540-231-2903, E-mail: dinman@vt.edu.

Contributed by the Technical Committee on Vibration and Sound for publication in the Journal of Vibration and Acoustics. Manuscript received April 2001; revised January 2002. Associate Editor: J. Wickert.

Finally, we conduct a parametric study to see the effects of aspect ratio (ratio of the two radii), pressure, and thickness on the natural frequencies.

2 Shell Geometry and Initial Stress Resultants

The middle surface of the toroidal shell is generated by the revolution of a circle of radius r with its center at a distance R $(=1/\kappa)$ from the axis of revolution (Fig. 1). Let ϕ and s be the curvilinear coordinates in the meridional and longitudinal directions, respectively, and let n be the radial direction. The Lamé parameters A_ϕ and A_s and the principal radii of curvatures R_ϕ and R_s are as follows (Plaut et al. [10]):

$$A_\phi = r, \quad A_s = 1 + r\kappa \cos\phi \tag{1}$$

$$R_\phi = r, \quad R_s = r + \frac{1}{\kappa \cos\phi} \tag{2}$$

The in-plane stress resultants N^r_ϕ, N^r_s, and $N^r_{\phi s} = N^r_{s\phi}$ (Fig. 2(*a*)) associated with the constant internal pressure p can be obtained by solving the following three equations (Budiansky [14]):

$$\frac{\partial(A_\phi N^r_s)}{\partial s} + \frac{\partial(A_s N^r_{\phi s})}{\partial \phi} + N^r_{\phi s}\frac{\partial A_s}{\partial \phi} - N^r_\phi \frac{\partial A_\phi}{\partial s} = 0 \tag{3}$$

$$\frac{\partial(A_s N^r_\phi)}{\partial \phi} + \frac{\partial(A_\phi N^r_{\phi s})}{\partial s} + N^r_{\phi s}\frac{\partial A_\phi}{\partial s} - N^r_s \frac{\partial A_s}{\partial \phi} = 0 \tag{4}$$

$$\frac{N^r_\phi}{R_\phi} + \frac{N^r_s}{R_s} = p \tag{5}$$

where p is the constant internal pressure. Since the toroidal shell and the loading due to the internal pressure are axisymmetric, Eqs. (3)–(5) can also be written in axisymmetric form. In order to solve the above static equations, we observe that due to this axisymmetric property $N^r_{\phi s} = 0$ and $\partial(\cdot)/\partial s = 0$. In addition, the stress resultants should be continuous along the tube. Using these conditions, the following expressions for the stress resultants can be obtained for a torus of constant circular cross-section:

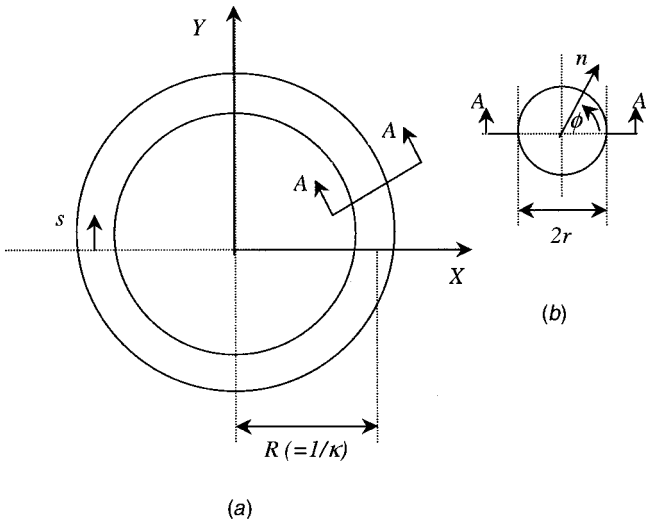

Fig. 1 Geometry of the torus (not to scale): (*a*) side view (*b*) section A-A

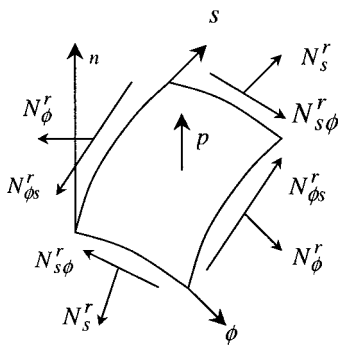

(*a*) Initial in-plane stress resultants and the pressure inside the torus

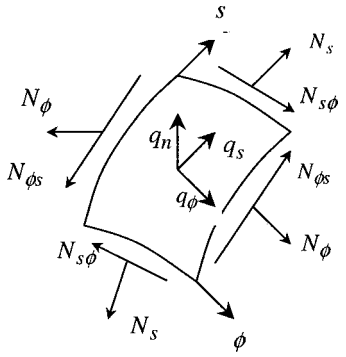

(*b*) In-plane stress resultants and external loadings

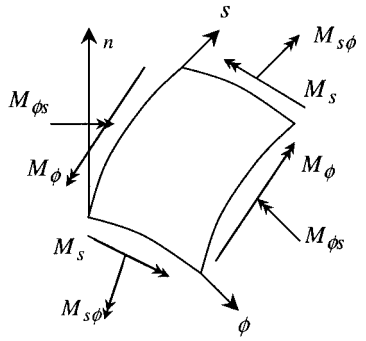

(*c*) Bending and twisting moment resultants

Fig. 2 Initial stresses, stress and moment resultants, and loads

$$N_{\phi}^{r}=\frac{pr}{2}\frac{(2+r\kappa\cos\phi)}{(1+r\kappa\cos\phi)},\quad N_{s}^{r}=\frac{pr}{2},\quad N_{\phi s}^{r}=0 \tag{6}$$

These initial in-plane stress resultants (N_{ϕ}^{r}, N_{s}^{r}, and $N_{\phi s}^{r}$) due to the internal pressure (p) are also called prestresses and will be used in the governing equations.

3 Governing Equations

3.1 Equilibrium. The in-plane stress resultants (N_{ϕ}, N_{s}, $N_{s\,\phi}$, and $N_{\phi s}$) and the bending and twisting moment resultants (M_{ϕ}, M_{s}, $M_{s\,\phi}$, and $M_{\phi s}$) are shown in Figs. 2(b) and 2(c) respectively. q_{ϕ}, q_{s}, and q_{n} are the surface traction forces per unit area along the ϕ, s, and n coordinates, respectively. The transverse shear resultants are not shown as they are replaced with equivalent expressions in the equilibrium equations. The modified membrane shear resultant and modified twisting moment resultant are defined as (Sanders [13])

$$\tilde{N}_{\phi s}=\frac{1}{2}(N_{\phi s}+N_{s\,\phi}),\quad \tilde{M}_{\phi s}=\frac{1}{2}(M_{\phi s}+M_{s\,\phi}), \tag{7}$$

respectively. Equilibrium equations including the prestresses (N_{ϕ}^{r}, N_{s}^{r}, and $N_{\phi s}^{r}$) are given by the following three equations (Budiansky [14]):

$$\begin{aligned}&\frac{\partial(N_{\phi}A_{s})}{\partial\phi}+\frac{\partial(\tilde{N}_{\phi s}A_{\phi})}{\partial s}+\tilde{N}_{\phi s}\frac{\partial A_{\phi}}{\partial s}-N_{s}\frac{\partial A_{s}}{\partial\phi}+\frac{1}{R_{\phi}}\frac{\partial(M_{\phi}A_{s})}{\partial\phi}\\&+\frac{1}{R_{\phi}}\frac{\partial\tilde{M}_{\phi s}A_{\phi}}{\partial s}+\frac{\tilde{M}_{\phi s}}{R_{\phi}}\frac{\partial A_{\phi}}{\partial s}-\frac{M_{s}}{R_{\phi}}\frac{\partial A_{s}}{\partial\phi}+\frac{A_{\phi}}{2}\frac{\partial}{\partial s}\\&\times\left(\tilde{M}_{\phi s}\left(\frac{1}{R_{\phi}}-\frac{1}{R_{s}}\right)\right)+A_{\phi}A_{s}N_{\phi}^{r}\left(\frac{1}{A_{\phi}}\frac{\partial\varepsilon_{\phi}}{\partial\phi}+\frac{\gamma_{\phi s}}{A_{\phi}A_{s}}\frac{\partial A_{\phi}}{\partial s}\right.\\&\left.-\frac{\beta_{\phi}}{R_{\phi}}\right)+2A_{\phi}A_{s}N_{\phi s}^{r}\left(\frac{1}{A_{s}}\frac{\partial\varepsilon_{\phi}}{\partial s}-\frac{\gamma_{\phi s}}{A_{\phi}A_{s}}\frac{\partial A_{s}}{\partial\phi}\right)\\&+A_{\phi}A_{s}N_{s}^{r}\left(\frac{1}{2A_{s}}\frac{\partial\gamma_{\phi s}}{\partial s}+\frac{(\varepsilon_{\phi}-\varepsilon_{s})}{A_{\phi}A_{s}}\frac{\partial A_{s}}{\partial\phi}-\frac{1}{A_{s}}\frac{\partial\beta_{n}}{\partial s}\right)\\&+p\beta_{\phi}A_{\phi}A_{s}=A_{\phi}A_{s}(\rho h\ddot{u}_{\phi}-q_{\phi})\end{aligned} \tag{8}$$

$$\begin{aligned}&\frac{\partial(N_{s}A_{\phi})}{\partial s}+\frac{\partial(\tilde{N}_{\phi s}A_{s})}{\partial\phi}+\tilde{N}_{\phi s}\frac{\partial A_{s}}{\partial\phi}-N_{\phi}\frac{\partial A_{\phi}}{\partial s}+\frac{1}{R_{s}}\frac{\partial(M_{s}A_{\phi})}{\partial s}\\&+\frac{1}{R_{s}}\frac{\partial\tilde{M}_{\phi s}A_{s}}{\partial\phi}+\frac{\tilde{M}_{\phi s}}{R_{s}}\frac{\partial A_{s}}{\partial\phi}-\frac{M_{\phi}}{R_{s}}\frac{\partial A_{\phi}}{\partial s}+\frac{A_{s}}{2}\frac{\partial}{\partial\phi}\\&\times\left[\left(\frac{1}{R_{s}}-\frac{1}{R_{\phi}}\right)\tilde{M}_{\phi s}\right]+A_{\phi}A_{s}N_{s}^{r}\left(\frac{1}{A_{s}}\frac{\partial\varepsilon_{s}}{\partial s}+\frac{\gamma_{\phi s}}{A_{\phi}A_{s}}\frac{\partial A_{s}}{\partial\phi}-\frac{\beta_{s}}{R_{s}}\right)\\&+2A_{\phi}A_{s}N_{\phi s}^{r}\left(\frac{1}{A_{\phi}}\frac{\partial\varepsilon_{s}}{\partial\phi}-\frac{\gamma_{\phi s}}{A_{\phi}A_{s}}\frac{\partial A_{\phi}}{\partial s}\right)+A_{\phi}A_{s}N_{\phi}^{r}\left(\frac{1}{2A_{\phi}}\frac{\partial\gamma_{\phi s}}{\partial\phi}\right.\\&\left.+\frac{(\varepsilon_{s}-\varepsilon_{\phi})}{A_{\phi}A_{s}}\frac{\partial A_{\phi}}{\partial s}+\frac{1}{A_{\phi}}\frac{\partial\beta_{n}}{\partial\phi}\right)+p\beta_{s}A_{\phi}A_{s}=A_{\phi}A_{s}(\rho h\ddot{u}_{s}-q_{s})\end{aligned} \tag{9}$$

$$\begin{aligned}&\frac{\partial}{\partial\phi}\left\{\frac{1}{A_{\phi}}\left[\frac{\partial(M_{\phi}A_{s})}{\partial\phi}+\frac{\partial(\tilde{M}_{\phi s}A_{\phi})}{\partial s}+\tilde{M}_{\phi s}\frac{\partial A_{\phi}}{\partial s}-M_{s}\frac{\partial A_{s}}{\partial\phi}\right]\right\}\\&+\frac{\partial}{\partial s}\left\{\frac{1}{A_{s}}\left[\frac{\partial(M_{s}A_{\phi})}{\partial s}+\frac{\partial(\tilde{M}_{\phi s}A_{s})}{\partial\phi}+\tilde{M}_{\phi s}\frac{\partial A_{s}}{\partial\phi}-M_{\phi}\frac{\partial A_{\phi}}{\partial s}\right]\right\}\\&-\left(\frac{N_{\phi}}{R_{\phi}}+\frac{N_{s}}{R_{s}}\right)A_{\phi}A_{s}-A_{\phi}A_{s}N_{\phi}^{r}\left(\frac{\varepsilon_{\phi}}{R_{\phi}}+\frac{1}{A_{\phi}}\frac{\partial\beta_{\phi}}{\partial\phi}+\frac{\beta_{s}}{A_{\phi}A_{s}}\frac{\partial A_{\phi}}{\partial s}\right)\\&-A_{\phi}A_{s}N_{\phi s}^{r}\left(\frac{1}{A_{s}}\frac{\partial\beta_{\phi}}{\partial s}+\frac{1}{A_{\phi}}\frac{\partial\beta_{s}}{\partial\phi}-\frac{\beta_{\phi}}{A_{\phi}A_{s}}\frac{\partial A_{\phi}}{\partial s}-\frac{\beta_{s}}{A_{\phi}A_{s}}\frac{\partial A_{s}}{\partial\phi}\right)\\&-\left(\frac{1}{R_{\phi}}-\frac{1}{R_{s}}\right)\beta_{n}+\left(\frac{1}{R_{\phi}}+\frac{1}{R_{s}}\right)\frac{\gamma_{\phi s}}{2}\Bigg)-A_{\phi}A_{s}N_{s}^{r}\left(\frac{\varepsilon_{s}}{R_{s}}+\frac{1}{A_{s}}\frac{\partial\beta_{s}}{\partial s}\right.\\&\left.+\frac{\beta_{\phi}}{A_{\phi}A_{s}}\frac{\partial A_{s}}{\partial\phi}\right)+A_{\phi}A_{s}p(\varepsilon_{\phi}+\varepsilon_{s})=A_{\phi}A_{s}(\rho h\ddot{w}-q_{n})\end{aligned} \tag{10}$$

where ρ is the density, β_{ϕ}, β_{s}, and β_{n} are the rotations defined in the next section, and $u_{\phi}(\phi,s,t)$, $u_{s}(\phi,s,t)$, and $w(\phi,s,t)$ are the mid-surface displacements in the ϕ, s, and n directions, respectively. In order to solve Eqs. (8)–(10), they are expressed in terms of the three mid-surface displacements. For a complete torus, the boundary conditions are simply the continuity conditions.

3.2 Strain-Displacement Relationships (Sanders [13]). Let ε_{ϕ} and ε_{s} be the in-plane extensional strains, and let κ_{ϕ} and be the bending strains. The in-plane shearing strain is $\gamma_{\phi s}$ and the twisting strains are $\kappa_{\phi s}$ and $\kappa_{s\phi}$. The modified twisting strain is defined as

$$\tilde{\kappa}_{\phi s}=\frac{1}{2}(\kappa_{\phi s}+\kappa_{s\phi}) \tag{11}$$

The rotations β_{ϕ}, β_{s}, and β_{n} are defined as

$$\begin{aligned}&\beta_{\phi}=\frac{u_{\phi}}{R_{\phi}}-\frac{1}{A_{\phi}}\frac{\partial w}{\partial\phi},\quad \beta_{s}=\frac{u_{s}}{R_{s}}-\frac{1}{A_{s}}\frac{\partial w}{\partial s},\\&\beta_{n}=\frac{1}{2A_{\phi}A_{s}}\left[\frac{\partial(A_{s}u_{s})}{\partial\phi}-\frac{\partial(A_{\phi}u_{\phi})}{\partial s}\right]\end{aligned} \tag{12}$$

The strain-displacement relationships are as follows:

$$\varepsilon_{\phi}=\frac{1}{A_{\phi}}\frac{\partial u_{\phi}}{\partial\phi}+\frac{1}{A_{\phi}A_{s}}\frac{\partial A_{\phi}}{\partial s}u_{s}+\frac{w}{R_{\phi}} \tag{13}$$

$$\varepsilon_{s}=\frac{1}{A_{s}}\frac{\partial u_{s}}{\partial s}+\frac{1}{A_{\phi}A_{s}}\frac{\partial A_{s}}{\partial\phi}u_{\phi}+\frac{w}{R_{s}} \tag{14}$$

$$\gamma_{\phi s}=\frac{1}{A_{\phi}A_{s}}\left(A_{s}\frac{\partial u_{s}}{\partial\phi}+A_{\phi}\frac{\partial u_{\phi}}{\partial s}-\frac{\partial A_{\phi}}{\partial s}u_{\phi}-\frac{\partial A_{s}}{\partial\phi}u_{s}\right) \tag{15}$$

$$\kappa_{\phi}=\frac{1}{A_{\phi}}\frac{\partial\beta_{\phi}}{\partial\phi}+\frac{1}{A_{\phi}A_{s}}\frac{\partial A_{\phi}}{\partial s}\beta_{s} \tag{16}$$

$$\kappa_{s}=\frac{1}{A_{s}}\frac{\partial\beta_{s}}{\partial s}+\frac{1}{A_{\phi}A_{s}}\frac{\partial A_{s}}{\partial\phi}\beta_{\phi} \tag{17}$$

$$\begin{aligned}\tilde{\kappa}_{\phi s}=\frac{1}{2}\Bigg\{&\left(\frac{1}{A_{\phi}}\frac{\partial\beta_{s}}{\partial\phi}+\frac{1}{A_{s}}\frac{\partial\beta_{\phi}}{\partial s}-\frac{\beta_{\phi}}{A_{\phi}A_{s}}\frac{\partial A_{\phi}}{\partial s}\right.\\&\left.-\frac{\beta_{s}}{A_{\phi}A_{s}}\frac{\partial A_{s}}{\partial\phi}+\beta_{n}\left(\frac{1}{R_{s}}-\frac{1}{R_{\phi}}\right)\right\}\end{aligned} \tag{18}$$

3.3 Constitutive Law. The material is assumed to be elastic and isotropic. The constitutive laws, which relate the stress measures to the strain measures, are given by the following equations (Sanders [13]):

$$N_{\phi}=K(\varepsilon_{\phi}+\nu\varepsilon_{s})\quad N_{s}=K(\varepsilon_{s}+\nu\varepsilon_{\phi})\quad \tilde{N}_{\phi s}=\frac{K(1-\nu)}{2}\gamma_{\phi s} \tag{19}$$

$$M_{\phi}=D(\kappa_{\phi}+\nu\kappa_{s})\quad M_{s}=D(\kappa_{s}+\nu\kappa_{\phi})\quad \tilde{M}_{\phi s}=D(1-\nu)\tilde{\kappa}_{\phi s} \tag{20}$$

where ν is Poisson's ratio and K and D are the membrane stiffness and the bending stiffness, respectively. K and D can be written in terms of Young's modulus (E), Poisson's ratio (ν), and the thickness of the shell (h) as follows:

$$K=\frac{Eh}{1-\nu^2},\quad D=\frac{Eh^3}{12(1-\nu^2)} \tag{21}$$

4 Solution Method

For the free vibration problem we drop the external loading terms in the Eqs. (8)–(10). The governing equations in terms of the displacement fields can be obtained by substituting the strain-displacement relationships, Eqs. (13)–(18), in the constitutive laws, Eqs. (19)–(20), and then substituting these stresses in the Eqs. (8)–(10). The resulting equations can be written in the following form:

$$l_{11}\{u_\phi\}+l_{12}\{u_s\}+l_{13}\{w\}-A_\phi A_s\rho h\ddot{u}_\phi=0 \tag{22}$$

$$l_{21}\{u_\phi\}+l_{22}\{u_s\}+l_{23}\{w\}-A_\phi A_s\rho h\ddot{u}_s=0 \tag{23}$$

$$l_{31}\{u_\phi\}+l_{32}\{u_s\}+l_{33}\{w\}-A_\phi A_s\rho h\ddot{w}=0 \tag{24}$$

where l_{ij} $(i,j=1,2,3)$ are the linear differential operators. For harmonic vibration we can eliminate the time dependency by writing

$$u_\phi(\phi,s,t)=U(\phi,s)e^{i\omega t},\quad u_s(\phi,s,t)=V(\phi,s)e^{i\omega t},\quad w(\phi,s,t)=W(\phi,s)e^{i\omega t} \tag{25}$$

where ω is the natural frequency. Assume that the displacement functions (U,V,W) can be separated spatially in the following forms:

$$U(\phi,s)=U_\phi(\phi)U_s(s),\quad V(\phi,s)=V_\phi(\phi)V_s(s),\quad W(\phi,s)=W_\phi(\phi)W_s(s) \tag{26}$$

The equilibrium equations can be reduced to a set of ordinary differential equations if the motion is assumed to be composed of complete waves in the form of sine and cosine functions in the longitudinal direction. To this end, we replace the displacement functions $U_s(s)$, $V_s(s)$, and $W_s(s)$ in Eq. (26) by either

$$U_s(s)=\sin\left(\frac{ns}{R}\right),\quad V_s(s)=-\cos\left(\frac{ns}{R}\right),\quad W_s(s)=\sin\left(\frac{ns}{R}\right) \tag{27}$$

or

$$U_s(s)=\cos\left(\frac{ns}{R}\right),\quad V_s(s)=\sin\left(\frac{ns}{R}\right),\quad W_s(s)=\cos\left(\frac{ns}{R}\right). \tag{28}$$

After above substitutions, we divide Eqs. (22), (23), and (24) by $U_s(s)$, $V_s(s)$, and $W_s(s)$, respectively. Here n, called the wave number, is an integer and $n\neq 0$. In fact, when $n\neq 0$, substitution of Eqs. (27) or (28) will yield the same natural frequencies but two independent mode shapes related to each other by a rotation. For $n=0$, Eqs. (27) and (28) will yield different natural frequencies. Mode shapes corresponding to $n=0$ in Eqs. (27) and (28) are called axisymmetric modes. The mode shapes corresponding to Eq. (27) and $n=0$ are also called dilationless circumferential modes or purely torsional modes. Now we can write Eqs. (22)–(24) as

$$l_{11\phi}\{U_\phi(\phi)\}+l_{12\phi}\{V_\phi(\phi)\}+l_{13\phi}\{W_\phi(\phi)\}+A_\phi A_s\rho h\omega^2U_\phi(\phi)=0 \tag{29}$$

$$l_{21\phi}\{U_\phi(\phi)\}+l_{22\phi}\{V_\phi(\phi)\}+l_{23\phi}\{W_\phi(\phi)\}+A_\phi A_s\rho h\omega^2V_\phi(\phi)=0 \tag{30}$$

$$l_{31\phi}\{U_\phi(\phi)\}+l_{32\phi}\{V_\phi(\phi)\}+l_{33\phi}\{W_\phi(\phi)\}+A_\phi A_s\rho h\omega^2W_\phi(\phi)=0 \tag{31}$$

where $l_{ij\phi}$ $(i,j=1,2,3)$ can be derived from l_{ij} using the above procedure. The resulting Eqs. (29)–(31) are linear differential equations with variable coefficients in ϕ and can be solved using Galerkin's method (Soedel [15], Leung and Kwok [7]). We can write the resulting equations in the following matrix form:

$$\mathbf{L}_\phi\mathbf{\Phi}+\lambda\mathbf{m}\mathbf{\Phi}=0 \tag{32}$$

where $\lambda=\omega^2$ and $\mathbf{L}_\phi$ is a matrix of the differential operators in ϕ. The matrices $\mathbf{L}_\phi$ and $\mathbf{m}$ and the displacement vector $\mathbf{\Phi}$ are given by

$$\mathbf{L}_\phi=\begin{bmatrix} l_{11\phi} & l_{12\phi} & l_{13\phi}\\ l_{21\phi} & l_{22\phi} & l_{23\phi}\\ l_{31\phi} & l_{32\phi} & l_{33\phi}\end{bmatrix},\quad \mathbf{m}=\begin{bmatrix} A_\phi A_s\rho h & 0 & 0\\ 0 & A_\phi A_s\rho h & 0\\ 0 & 0 & A_\phi A_s\rho h\end{bmatrix},\quad \mathbf{\Phi}=\begin{Bmatrix} U_\phi(\phi)\\ V_\phi(\phi)\\ W_\phi(\phi)\end{Bmatrix} \tag{33}$$

We consider the integral statement of the system of differential equations:

$$\int_\Omega[\mathbf{\Phi}_a^T\mathbf{L}_\phi\mathbf{\Phi}+\lambda\mathbf{\Phi}_a^T\mathbf{m}\mathbf{\Phi}]d\Omega=0 \tag{34}$$

where Ω is the domain in which the system of differential equations is to be satisfied, $\mathbf{\Phi}_a$ is an arbitrary weighting function vector, and the superscript T denotes the transpose of a matrix. Choosing the arbitrary weighting function $\mathbf{\Phi}_a$ as a variation of $\mathbf{\Phi}$, denoted by $\boldsymbol{\delta\Phi}$, we get

$$\int_0^{2\pi}[\boldsymbol{\delta\Phi}^T\mathbf{L}_\phi\mathbf{\Phi}+\lambda\boldsymbol{\delta\Phi}^T\mathbf{m}\mathbf{\Phi}]d\phi=0 \tag{35}$$

McGill [4] showed that the deflection function of a torus could be constructed of solutions such that either

(a) $V(\phi,s)$ and $W(\phi,s)$ are even and $U(\phi,s)$ is odd with respect to $\phi=0$ and π, or
(b) $V(\phi,s)$ and $W(\phi,s)$ are odd and $U(\phi,s)$ is even with respect to $\phi=0$ and π.

The modes of type (a) are called symmetric modes, because they yield a symmetric picture of a meridional cross-section with respect to $\phi=0$ and π (Fig. 3(*a*)). Similarly, mode shapes of type (b) are denoted as antisymmetric modes because of the antisymmetric pattern with respect to $\phi=0$ and π (Fig. 3(*b*)). These two groups of vibration modes can be analyzed independently. It is also evident that the displacement function must be a continuous periodic function with continuous periodic derivatives of the same period in ϕ. Hence $U_\phi(\phi)$, $V_\phi(\phi)$, and $W_\phi(\phi)$ can be represented by Fourier series. Taking a finite number of terms (m) in the Fourier series, we can write the symmetric part as

$$U_\phi^s(\phi)=\sum_{i=1}^{m}A_i^s\sin(i\phi)\quad V_\phi^s(\phi)=\sum_{i=0}^{m-1}B_i^s\cos(i\phi)\quad W_\phi^s(\phi)=\sum_{i=0}^{m-1}C_i^s\cos(i\phi) \tag{36}$$

where superscript s denotes the symmetric part. Similarly, we can write the antisymmetric part as

$$U_\phi^a(\phi)=\sum_{i=0}^{m-1}A_i^a\cos(i\phi)\quad V_\phi^a(\phi)=\sum_{i=1}^{m}B_i^a\sin(i\phi)\quad W_\phi^a(\phi)=\sum_{i=1}^{m}C_i^a\sin(i\phi) \tag{37}$$

where superscript a denotes the antisymmetric part. Thus the vector $\mathbf{\Phi}$ can be written as

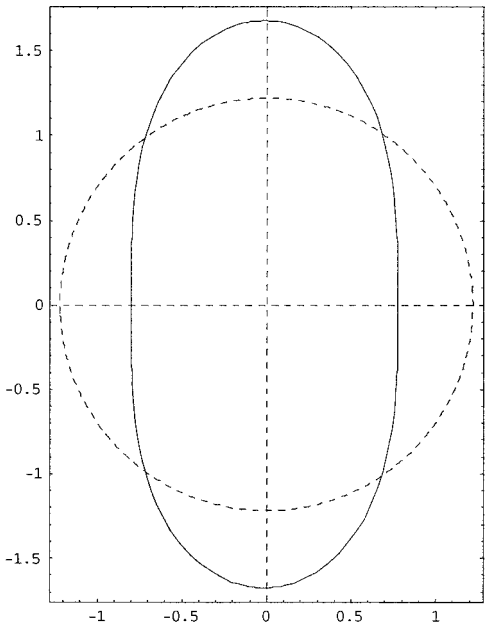

(*a*) Symmetric deformation

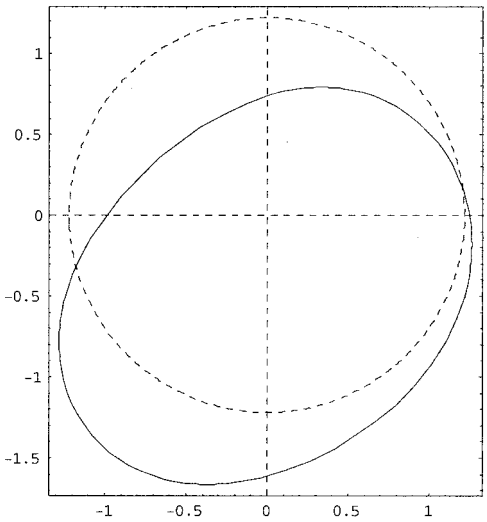

(*b*) Antisymmetric deformation

Fig. 3 Symmetrically and antisymmetrically deformed cross-sections of the torus. Solid lines are the deformed cross-sections and dotted lines are the undeformed cross-sections and axes.

$$\mathbf{\Phi}=\mathbf{fa} \tag{38}$$

where **a** is the vector of unknown coefficients A_i^s, B_i^s, and C_i^s in the symmetric case, A_i^a, B_i^a, and C_i^a in the antisymmetric case ($i=1,2,...m$), and **f** is a matrix so that **f a** gives the displacement vector $\mathbf{\Phi}$ in Eq. (38). Now we can write Eq. (35) as

$$\int_0^{2\pi}[\,\delta\mathbf{a}^T\mathbf{f}^T\mathbf{L}_\phi\mathbf{fa}+\lambda\,\delta\mathbf{a}^T\mathbf{f}^T\mathbf{mfa}]d\phi=0 \tag{39}$$

Since $\delta\mathbf{a}$ is arbitrary, we have

$$\int_0^{2\pi}[\mathbf{f}^T\mathbf{L}_\phi\mathbf{fa}+\lambda\mathbf{f}^T\mathbf{mfa}]d\phi=0 \tag{40}$$

The above equation after integration can be written in the following matrix form:

$$(\mathbf{A}+\lambda\mathbf{B})\mathbf{a}=0 \tag{41}$$

where the matrices **A** and **B** are given by

$$\mathbf{A}=\int_0^{2\pi}\mathbf{f}^T\mathbf{L}_\phi\mathbf{f}d\phi,\quad \mathbf{B}=\int_0^{2\pi}\mathbf{f}^T\mathbf{mf}d\phi \tag{42}$$

Equation (41) is an eigenvalue problem. The eigenvalue λ is the square of the natural frequency, and the eigenvector **a** gives the vibration mode shape.

5 Numerical Result

Now we present a few numerical examples to demonstrate the method described above. The frequencies mentioned in this section are non-rigid-body frequencies. The rigid-body frequencies are described in the next section.

5.1 Cylindrical Shell. First, we consider a special case of torus where the radius R of the torus (Fig. 1(*a*)) becomes very large compared to the radius r of the cross-section of the torus, so that the geometry of the toroidal shell becomes close to that of a circular cylinder. For this special case, we also assume that the internal pressure (p) is zero (Table 1). The results are compared with the exact natural frequencies (Leissa [16]). The shear diaphragm boundary condition is assumed. The length of the cylinder is taken to be πR so that the boundary conditions are satisfied exactly by the displacement function in the longitudinal direction (Eq. (27)). Table 2 shows the natural frequencies calculated using this analysis and the exact solution. Since the exact solution was also obtained using Sanders' theory, the results show perfect agreement. In this case, the symmetric and antisymmetric vibrations give the same natural frequencies. This is because a circular cylinder possesses symmetry in the meridional direction and hence the symmetric and antisymmetric modes are related to each other simply by a rotation. However, some vibration modes, e.g., torsional vibration modes, can only be predicted by antisymmetric modes. Since every term in the displacement function (Eqs. (36) and (37)) constitutes a mode shape for a circular cylinder, the convergence is independent of the number of terms taken in the series.

5.2 Toroidal Shell. In this section, we present the natural frequencies and mode shapes of an inflated torus. First, we compare the natural frequencies with those given in Liepins [11]. The results will be shown in terms of the following nondimensional quantities:

$$\eta=\frac{r}{R},\quad \zeta=\frac{pr}{Eh},\quad \mu=\frac{\rho r^2}{E\,\eta^2}\,\omega^2 \tag{43}$$

where η, ζ, and μ denote the aspect ratio, prestress parameter, and frequency parameter, respectively. Table 3 shows values of μ when $\eta=0.3$ and $\zeta=0.002$ for different wave numbers. The natural frequency shown corresponds to the first mode in each case. The results match closely. The reasons for the small differences may be numerical inaccuracies or the fact that Liepins [11] uses a finite difference method whereas we use Fourier series.

Table 1 Data for the geometry and material of the cylinder

Parameter	Values
Elastic modulus E, Pa	2.07×10^{11}
Thickness h, m	0.01
Poisson's ratio ν	0.3
Density ρ, kg/m^3	7800
Length L, m	7.62
Radius of the cross-section r, m	1.219

Table 2 Comparison of natural frequencies for the cylinder

Mode number	Axial wave number, circumferential wave number (n, i)	Frequency from this analysis (Hz)	Exact values (Hz) (Leissa [16])
1	1, 2	5.91	5.91
2	1, 1	11.76	11.76
3	1, 3	12.83	12.83
4	2, 3	14.67	14.67
5	2, 2	15.65	15.65
6	3, 3	20.52	20.52
7	1, 4	24.35	24.35

Table 3 Comparison of natural frequencies for the inflated torus (η=0.3 and ζ=0.002)

Wave number (n), Symmetry (First mode)	Frequency parameter from this analysis (μ)	Frequency parameter from Liepins [11] (μ)
0, symmetric	0.40	0.39
0, antisymmetric	0.04	0.04
1, symmetric	0.39	0.38
1, antisymmetric	0.23	0.23
2, symmetric	0.05	0.05
2, antisymmetric	0.04	0.04

The above two comparisons demonstrate that the results from this analysis are accurate. Following a similar procedure, one can also calculate the natural frequencies and mode shapes for the torus without pressure by setting all the prestress and pressure terms in the governing equations to zero.

A candidate for the material of an inflatable structure is Kapton ®. Since an inflatable structure is the main interest of this work, we use this material for the analysis hereafter. Table 4 shows the data for the geometry and material of the inflatable torus.

The mode shapes and the corresponding natural frequencies are shown in Figs. 4 and 5. These figures also show the projections of mode shapes on a plane. Modes 1, 4, and 7 are the out-of-plane bending modes. These modes resemble the bending modes of a free-free beam and produced by the antisymmetric modes. Also, the modes 3, 6, 10, and 11 are of antisymmetric type. Modes 2, 5, 8, 9, and 12 are symmetric modes. In mode 2, the torus vibrates by forming elliptical shape. Similarly, in modes 5 and 9, it forms triangular and square shape. Modes 3 and 8 are axisymmetric modes. In an axisymmetric mode, the shape does not change along θ, but the cross-section deforms either antisymmetrically, called the axisymmetric antisymmetric mode (mode 3), or symmetrically, called the axisymmetric symmetric mode (mode 8). The complexities of mode shapes increase with an increase in the aspect ratio (r/R). For a low aspect ratio torus, the ring types of modes dominate the lower modes. On the other hand, for a torus of very high aspect ratio, the local deformation of the meridional curve (cross-section) dominates even in the lower modes. We also note that since the thickness of the structure is very small, bending moments in the governing equations can be neglected since they are very small compared to the in-plane stresses.

Now we consider the effects of various quantities on the natural frequencies of the inflated torus. Parameters, one at a time, will be changed from the values given in Table 4, and the corresponding frequencies will be calculated and plotted. To study the effect of the aspect ratio, we consider frequencies at a low wave number ($n=0$) and at a high wave number ($n=4$). Figure 6 shows the changes in natural frequencies as the aspect ratio (r/R) of the torus changes for the case of $n=0$. As the aspect ratio increases, frequencies decrease. It can be seen that the rate of decrease is very high up to an aspect ratio of 0.1. Also, the symmetric and antisymmetric frequencies are close to each other except for the first frequency at low aspect ratios. Compared to the frequencies at a low aspect ratio, we see that the frequencies are more closely spaced at a high aspect ratio. Basically, at high aspect ratio the natural frequencies occur in clusters and the there are several modes near any frequency. On the other hand, for low aspect ratio the natural frequencies and mode shapes are widely separated. Figure 7 shows the plot of the natural frequencies against the aspect ratio for $n=4$. Unlike the frequencies for $n=0$, we see that the first frequency of both the symmetric and the antisymmetric modes increases up to an aspect ratio of around 0.26. Again, at low aspect ratio the frequencies are wide apart contrary to the behavior at high aspect ratio. Figure 8 shows the effect of pressure (p) on the natural frequencies. As expected, the frequencies increase with the internal pressure. This is because of the increase in

Table 4 Data for the geometry and material of the torus

Parameter	Values
Elastic modulus E, N/m^2	2.55×10^{9}
Thickness h, m	76.2×10^{-6}
Poisson's ratio ν	0.34
Density ρ, kg/m^3	1418
Radius of torus R, m	7.62
Radius of the cross-section r, m	1.22
Internal pressure p, N/m^2	1723.69

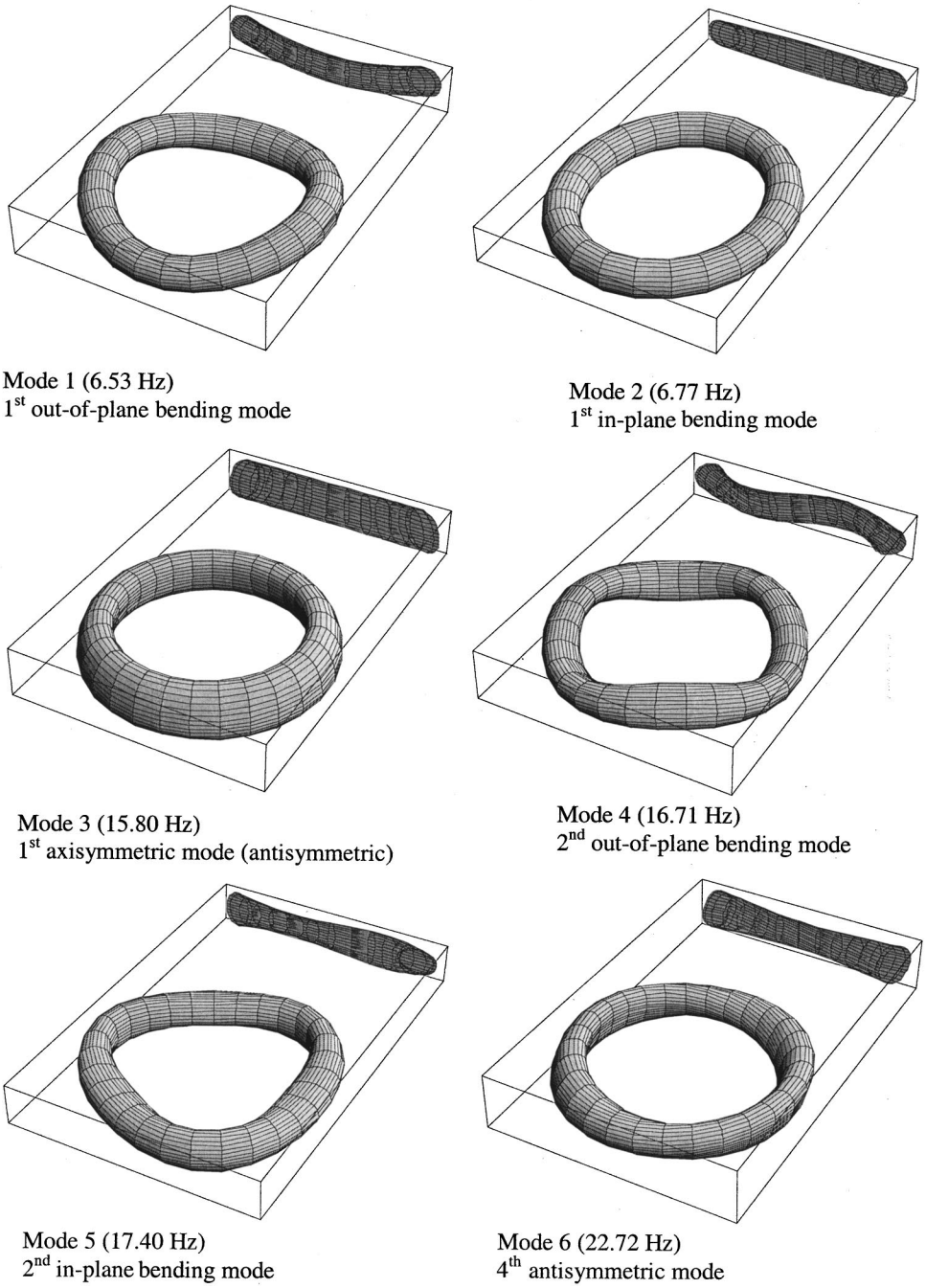

Fig. 4 Mode shapes of the inflated torus

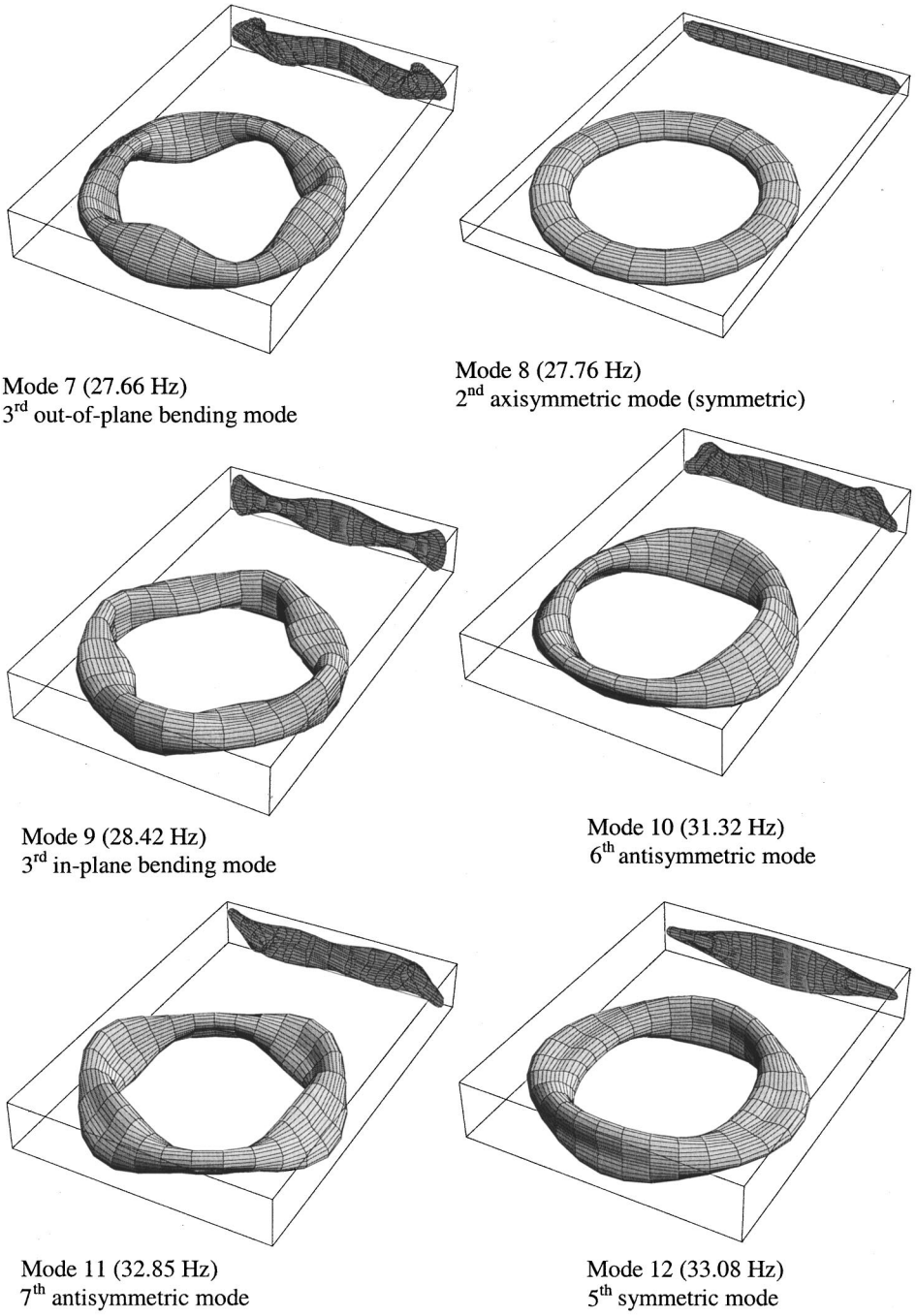

Fig. 5 Mode shapes of the inflated torus

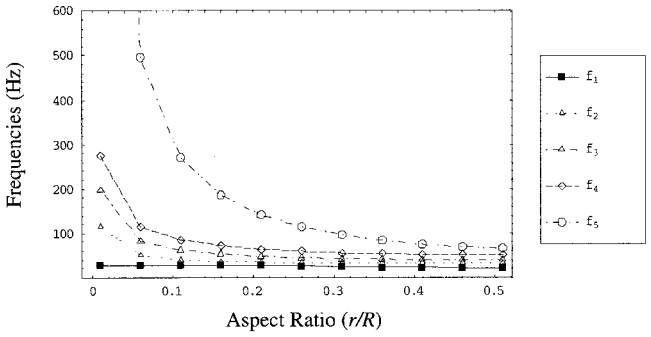

(*a*) Frequencies of symmetric modes for $n = 0$

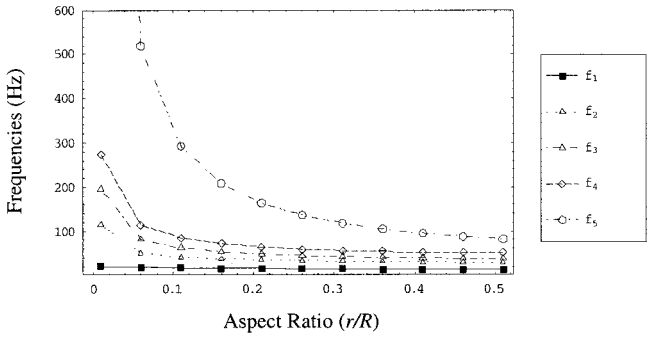

(*b*) Frequencies of antisymmetric modes for $n = 0$

Fig. 6 The first five natural frequencies vs. the aspect ratio of (*a*) symmetric modes and (*b*) antisymmetric modes corresponding to $n=0$

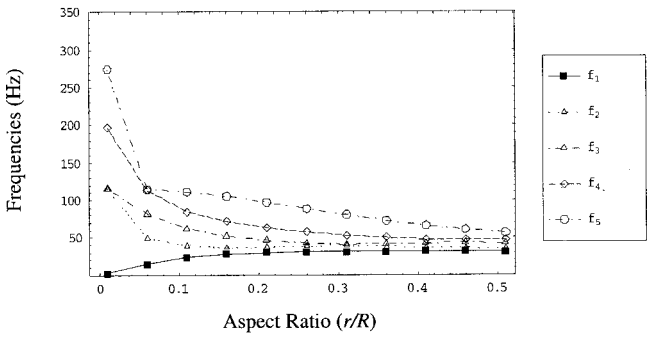

(*a*) Frequencies of symmetric modes for $n = 4$

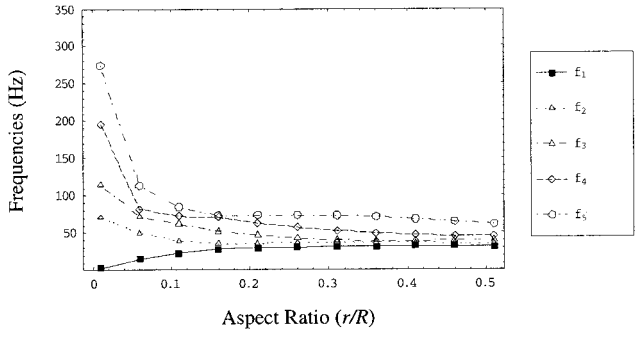

(*b*) Frequencies of antisymmetric modes for $n = 4$

Fig. 7 The first five natural frequencies vs. the aspect ratio of (*a*) symmetric modes and (*b*) antisymmetric modes corresponding to $n=4$

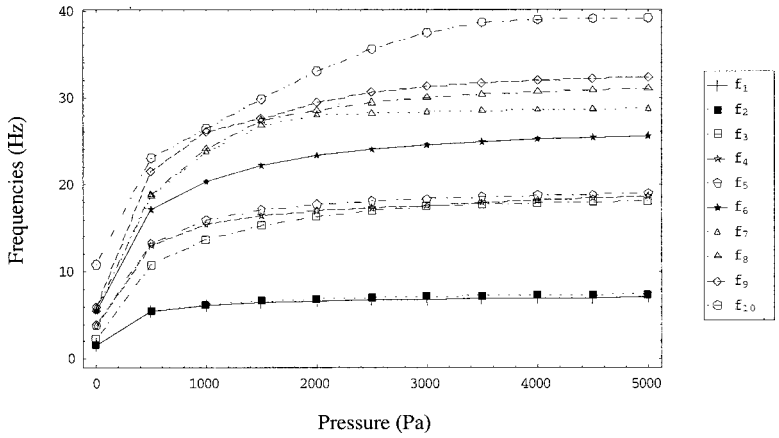

Fig. 8 Effect of the internal pressure on the first ten natural frequencies of the inflated torus

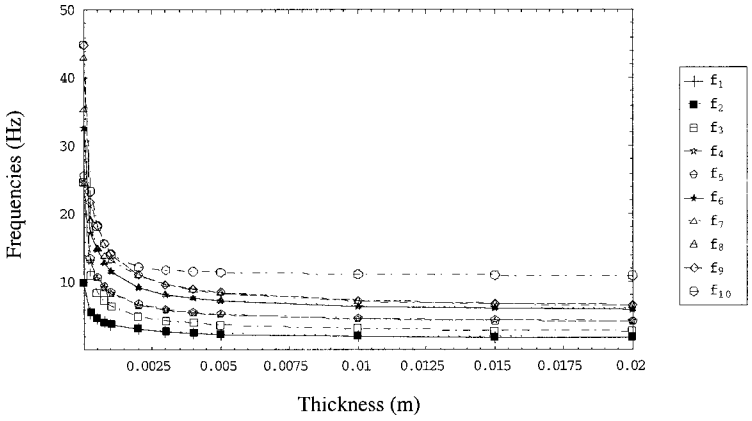

Fig. 9 Effect of the thickness on the first ten natural frequencies of the inflated torus

stiffness with the increase in pressure. In an inflatable structure, the major source of the stiffness is its internal pressure. The rate of increase in the frequencies is not constant throughout the pressure range. First the natural frequencies increase rapidly, and thereafter they increase slowly or remain nearly constant. Figure 9 is a plot of the natural frequencies vs. thickness (t) of the torus. Initially the frequencies decrease quickly and later they decrease slowly with the wall thickness of the torus.

6 Rigid-Body Modes

Since the boundary conditions of the inflated torus are free, it shows six rigid-body modes corresponding to six zero natural frequencies. Of the six rigid body motions, three are translations and the other three are the rotations about the three perpendicular axes. It is worth noting here that one of the main advantages of using Sanders' shell theory is that, unlike Love's shell theory, strains do vanish for all six small rigid-body motions. The following displacement functions give rise to the rigid body modes (Kordes [3]):

(a) Displacement parallel to the axis of symmetry:

$$U(\phi,s)=A\cos(\phi),\quad V(\phi,s)=0,\quad W(\phi,s)=A\sin(\phi) \tag{44}$$

(b) Displacement perpendicular to the axis of symmetry:

$$U(\phi,s)=A\sin(\phi)\sin(s/R),\quad V(\phi,s)=-A\cos(s/R),$$
$$W(\phi,s)=-A\cos(\phi)\sin(s/R) \tag{45}$$

$$U(\phi,s)=A\sin(\phi)\cos(s/R),\quad V(\phi,s)=-A\sin(s/R),$$
$$W(\phi,s)=-A\cos(\phi)\cos(s/R), \tag{46}$$

(c) Rotation about the axis of symmetry:

$$U(\phi,s)=0,\quad V(\phi,s)=A\{R+r\cos(\phi)\},\quad W(\phi,s)=0 \tag{47}$$

(d) Rotation about axes perpendicular to the axis of symmetry

$$U(\phi,s)=A\{r+R\cos(\phi)\}\sin(s/R),$$
$$V(\phi,s)=-Ar\sin(\phi)\cos(s/R),\quad W(\phi,s)=AR\sin(\phi)\sin(s/R) \tag{48}$$

$$U(\phi,s)=A\{r+R\cos(\phi)\}\cos(s/R),$$
$$V(\phi,s)=-Ar\sin(\phi)\sin(s/R),$$
$$W(\phi,s)=-AR\sin(\phi)\cos(s/R), \tag{49}$$

Using the above rigid-body modes, the zero natural frequencies were verified.

7 Conclusions

The free vibration analysis of an inflated torus with free boundary conditions has been presented. The governing equations were formulated using Sanders' shell theory including the effect of pressure. The displacement functions were assumed to consist of complete sine and cosine waves in the longitudinal direction. This reduces the governing partial differential equations to a set of ordinary differential equations in the meridional coordinate ϕ, which was solved using Galerkin's method to obtain the mode shapes and the natural frequencies. The displacement functions in ϕ were written in two groups, called the symmetric and antisymmetric modes, using Fourier series. First, we calculated the natural frequencies for a cylinder without pressure, which is a special case. The results were found to match the exact solution. Then the case of an inflated torus was considered and the results were again compared with existing ones. The mode shapes and natural frequencies were presented. Finally, a parametric study was done to show the effects of the aspect ratio, pressure, and thickness on the natural frequencies corresponding to different mode shapes. The natural frequencies were found to be mostly decreasing with an increase in thickness and aspect ratio. However, with an increase in pressure, the frequencies were found to be increasing. In all these cases, the change is high initially and then it becomes slow.

Acknowledgments

This work was sponsored by the Air Force Office of Scientific Research under grant number F49620-99-1. The authors are also grateful to Dr. Eric Johnson and Dr. Rakesh Kapania of the Department of Aerospace and Ocean Engineering for helpful discussions.

References

[1] Malone, P. K., and Crawford, L., 1993, "Developing an Inflatable Solar Array," *7th AIAA/USU Conference on Small Satellites*, LPA-93-GW-008, P1J93.
[2] Dornheim, M. A., 1999, "Inflatable Structures Taking to Flight," Aviat. Week Space Technol., January, pp. 60–62.
[3] Kordes, E. E., 1960, "Vibration Analysis of Toroidal Shells of Circular Cross Section," Ph.D. Dissertation, Engineering, Mechanics, Virginia Polytechnic Institute and State University, Blacksburg, VA.
[4] McGill, D. J. M., 1966, "Axisymmetric Free Oscillations of Thick Toroidal Shells," Ph.D. Dissertation, Department of Mechanics and Aerospace Engineering, University of Kansas, Lawrence, KS.
[5] Kosawada, T., Suzuki, K., and Takahashi, S., 1985, "Free Vibration of Toroidal Shells," Bull. JSME, **28**(243), pp. 2041–2047.
[6] Fang, Z., 1992, "Free Vibration of Fluid-Filled Toroidal Shells," J. Sound Vib., **155**(2), pp. 343–352.
[7] Leung, A. Y. T., and Kwok, N. T. C., 1994, "Free Vibration Analysis of a Toroidal Shell," Thin-Walled Struct., **18**, pp. 317–332.
[8] Jordan, P. F., 1966, "Vibration and Buckling of Pressurized Torus Shells," *4th Aerospace Science Meeting*, Los Angeles, California, AIAA Paper No. 66–445.
[9] Saigal, S., Yang, T. Y., Kim, H. W., and Soedel, W., 1986, "Free Vibration of a Tire as a Toroidal Membrane," J. Sound Vib., **107**(1), pp. 71–82.
[10] Plaut, R. H., Goh, J. K. S., Kigudde, M., and Hammerand, D. C., 2000, "Shell Analysis of an Inflatable Arch Subjected to Snow and Wind Loading," Int. J. Solids Struct., **37**, pp. 4275–4288.
[11] Liepins, A. A., 1965, "Free Vibrations of Prestressed Toroidal Membrane," AIAA J., **3**(10), pp. 1924–1933.
[12] Lewis, J. A., 2000, "Finite Element Modeling and Active Control of an Inflated Torus Using Piezoelectric Devices," MS Thesis, Mechanical Engineering, Virginia Polytechnic Institute and State University, Blacksburg, VA.
[13] Sanders, J. L., 1959, "An Improved First Approximation Theory for Thin Shells," NASA Report 24, June, Washington, D.C.
[14] Budiansky, B., 1968, "Notes on Nonlinear Shell Theory," ASME J. Appl. Mech., June, pp. 393–401, **35**, No. 2.
[15] Soedel, W., 1986, *Vibrations of Shells and Plates*, Marcel Dekker, New York.
[16] Leissa, A. W., 1973, *Vibration of Shells*, NASA SP-288, Washington, D.C.